division multiplexing (PDM), the spectral efficiency of DQPSK signals is more than 2 b/s/Hz (Cho et al., 2004a,b).

1. Generation of Multilevel Signals

From the low-pass representation of the signal of $A_s(t)e^{j\phi_s(t)}$, there are many methods to generate multilevel signal. In an M-ary PSK signal, the phase is divided into M evenly levels for M different waveforms. In an M-ary QAM signal, both the amplitude of $A_s(t)$ and the phase of $\phi_s(t)$ are used for M different waveforms. While there are other variations to use M different frequencies or only a real number of both positive and negative $A_s(t)$, those methods usually do not provide better spectral efficiency than M-ary QAM signals. For superior spectral efficiency, we focus on both M-ary PSK and QAM signals.

An M-ary PSK signal has a constant amplitude of $A_s(t) = A$ and M evenly spacing phases of $\theta_k = \pi(2k-1)/M$, $k = 1, 2, \ldots, M$. The M different signal waveforms are

$$\begin{aligned} s_k(t) &= \Re\left\{Ae^{j\pi(2k-1)/M}e^{j\omega_c t}\right\}, \\ &= A\cos\left[\frac{\pi(2k-1)}{M}\right]\cos\omega_c t - A\sin\left[\frac{\pi(2k-1)}{M}\right]\sin\omega_c t, \\ &\qquad k = 1, 2, \ldots, M. \end{aligned} \tag{9.1}$$

The Euclidean distance between the k and lth symbols is equal to

$$\sqrt{2}A\left|\sin\left(\frac{(k-l)\pi}{M}\right)\right| \tag{9.2}$$

with a minimum Euclidean distance of $\sqrt{2}A\sin\pi/M$.

Both quadrature phase-shift keying (QPSK) and DQPSK systems use the waveforms of Eq. (9.1) with $M = 4$ to transmit four possible different phases in a single time interval. Currently, most spectral efficiency systems use DQPSK signals as from Table 1.3. Figure 9.1 shows the constellation of (D)QPSK signals with normalized constellation points of

$$\pm 1 \pm j. \tag{9.3}$$

Like the same transmitted signal for binary PSK and DPSK signals, QPSK and DQPSK systems transmit the same signal. QPSK signal uses synchronous receiver based on the quadrature receiver of Fig. 3.4. DQPSK signal uses an asynchronous receiver similar to the DPSK receiver of Figs. 1.4(b) and (c). DQPSK signal requires a precoder to eliminate error propagating in the receiver but QPSK signal typically

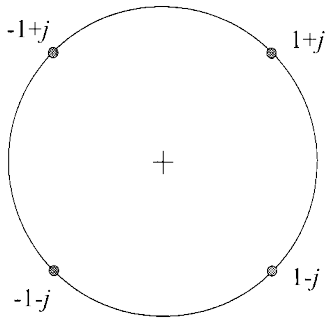

Figure 9.1. The constellation of (D)QPSK signals

does not require a precoder. The design of DQPSK precoder is considered later.

QAM signal provides the highest spectral efficiency among all types of modulation scheme. In an M-ary QAM systems, if $\sqrt{M}$ is an integer, the M different signal waveforms are

$$\begin{aligned} s_k(t) &= A\Re\left\{(a_k + jb_k)e^{j\omega_c t}\right\} \\ &= a_k A\cos\omega_c t - b_k A\sin\omega_c t, \\ &\quad a_k, b_k = -\sqrt{M}+1, -\sqrt{M}+3, \ldots, -1, +1, \ldots, \sqrt{M}-1. \end{aligned} \tag{9.4}$$

Figure 1.6 shows a 64-QAM constellation in a square grid. For simplicity, we assume that all 64 points are used and transmit with equal probability. In general, QAM constellation may locate in irregular location for optimal performance (Foschini et al., 1974, Gockenbach and Kearsley, 1999). M-ary PSK signal can be considered as a special case of QAM signal. Different constellation point of a QAM signal also does not necessary to transmit in the same probability. The system may achieve better performance with unequal probability for different constellation point by signal shaping (Calderbank and Ozarow, 1990, Laroia et al., 1994).

This section discusses two methods that generate QAM signal based on special (usually integrated) modulator or conventional dual-drive Mach-Zehnder modulator of Fig. 2.13. The generation of QAM signal is used as an example.

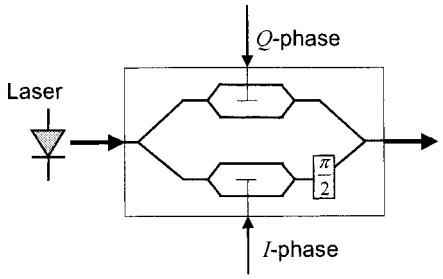

Figure 9.2. QAM transmitter based on two Mach-Zehnder modulators in an interferometer. [From Ho and Cuei (2005), © 2005 IEEE]

1.1 Conventional Quadrature Signal Generator

Figure 9.2 shows a conventional QAM transmitter based on two Mach-Zehnder modulators within an interferometer. A QAM signal can be represented as

$$s(t) = a(t)\cos\omega_c t + b(t)\sin\omega_c t, \tag{9.5}$$

where $a(t)$ and $b(t)$ are the two independent quadrature signals and ω_c is the angular frequency of the optical carrier. Compared Eq. (9.4) and (9.5), $a(t)$ and $b(t)$ are one of the $a_k A$ and $-b_k A$, $m = 1, 2, \ldots, M$ that change from time to time to encode digital data. The transmitter of Fig. 9.2 is the direct generation of the quadrature signals of Eq. (9.5). For the 64-QAM rectangular constellation of Fig. 1.6, $a(t)$ and $b(t)$ are both eight-level signals.

The two Mach-Zehnder modulators of Fig. 9.2 generate the signal for the two quadrature components with a phase difference of $\pi/2$, i.e., cosine and sine. If the upper branch of Fig. 9.2 has a carrier of $\cos\omega_c t$, with 90° phase difference, the lower branch has a carrier of $-\sin\omega_c t$. The baseband complex representation of the output of the transmitter of Eq. (9.5) is the complex number of $a(t) + b(t)e^{-j\pi/2} = a(t) - jb(t)$. The two Mach-Zehnder modulators of Fig. 9.2 should have zero chirp. From the transfer characteristic of Eq. (2.51), both modulators should operate with a peak-to-peak drive voltage of $2V_\pi$ such that both $a(t)$ and $b(t)$ can be both positive and negative values with minimum signal loss. The output electric field is thus

$$E_o = \Re\{[a(t) - jb(t)]e^{j\omega_c t}\} = a(t)\cos(\omega_c t) + b(t)\sin(\omega_c t), \tag{9.6}$$

the same as Eq. (9.5), where $\Re\{\cdot\}$ denotes the real part of a complex number. The signal of $a(t)$ and $b(t)$ of Eqs. (9.5) and (9.6) are from the two independent drive signals of the two Mach-Zehnder modulators of

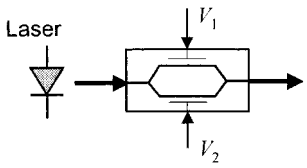

Figure 9.3. Basic structure of a dual-drive Mach-Zehnder modulator with two independent phase modulators in a Mach-Zehnder interferometer.

$V_1(t)$ and $V_2(t)$ in Fig. 9.2. Due to the nonlinear transfer characteristic of Eq. (2.51), the driving voltages of $V_1(t)$ and $V_2(t)$ are not necessary evenly spacing for evenly spacing signal of Eq. (9.5).

With two Mach-Zehnder modulators and an interferometer, the special modulator of Fig. 9.2 is difficult to fabricate. If the transmitter of Fig. 9.2 is implemented using discrete components of two Mach-Zehnder modulators within an interferometer, the transmitter is costly with many components. The transmitter in Fig. 9.2 also requires two bias controls for the Mach-Zehnder modulators and a phase control of the $\pi/2$ phase shifter. Most DQPSK demonstrations of Griffin and Carter (2002), Griffin et al. (2003), Zhu et al. (2004b), and Cho et al. (2003, 2004a,b) use an integrated transmitter the same as that shown in Fig. 9.2. The conventional QAM transmitter may be fabricated using electro-optic effect in semiconductor (Griffin et al., 2002, 2003, 2004) or $LiNbO_3$ (Cho et al., 2004b). As shown later, QAM signal can also be generated using a single dual-drive Mach-Zehnder modulator of Fig. 2.13.

1.2 Generation of QAM Signal Using a Single Dual-Drive Modulator

A QAM signal can also be generated using a conventional dual-drive Mach-Zehnder modulator. Figure 9.3 is the basic structure of a dual-drive Mach-Zehnder modulator, the same as that of Fig. 2.13. The dual-drive Mach-Zehnder modulator consists of two phase modulators that can be operated independently.

As shown in Sec. 2.3.2, Mach-Zehnder modulator can be made using various materials and $LiNbO_3$ is the most popular material. Almost all commercial long-haul dense wavelength-division-multiplexed (WDM) systems use $LiNbO_3$ Mach-Zehnder modulator. In the dual-drive structure of Fig. 9.3, the modulator chirp is adjustable (Gnauck et al., 1991, Ho and Kahn, 2004c). Currently, dual-drive 40 Gb/s modulator with a V_π of less than 2 V has been fabricated (Sugiyama et al., 2002).

For simplicity, assume an operation in steady-state for the modulator. Similar to Eq. (2.51) but the two paths of the dual-drive Mach-Zehnder modulator have independent drive voltages of V_1 and V_2, with an input electric field of E_i, the output electric field is,

$$E_o = \frac{E_i}{2}\left[\exp\left(j\pi\frac{V_1}{V_\pi}\right) + \exp\left(j\pi\frac{V_2}{V_\pi}\right)\right], \tag{9.7}$$

where V_π is the voltage to provide a 180° phase shift of each phase modulator. In the most trivial case, the Mach-Zehnder modulator is operated as a phase modulation if $V_1 = V_2$. The input and output relationship of Eq. (9.7) is rewritten in the following normalized form of

$$E_o = \frac{r_{\max}}{2}\left(e^{j\phi_1} - e^{j\phi_2}\right), \tag{9.8}$$

where $\phi_1 = \pi V_1/V_\pi$ and $\phi_2 = \pi V_2/V_\pi + \pi$. The output electric field of E_o is the difference of two vectors in the circle having a radius of $r_{\max}/2$. The modulator of Eq. (9.8) is biased at the minimum transmission point or the null point and the maximum output electric field has an amplitude of $r_{\max}$ when $V_1 = V_2$ or ϕ_1 and ϕ_2 are antipodal phases. The representation of Eq. (9.8) gives a simple geometric representation of the operation of a dual-drive Mach-Zehnder modulator with two independent phase modulators.

Assumed an M-ary signal constellation that can be represented as complex numbers of

$$s_k = r_k e^{j\theta_k}, \quad r_k > 0, \quad 0 \le \theta_k < 2\pi, \qquad k = 0, \ldots, M-1, \tag{9.9}$$

with maximum amplitude of

$$r_{\max} = \max\{r_0, r_1, \ldots, r_{M-1}\}. \tag{9.10}$$

With two phases of

$$\phi_{k1} = \theta_k + \cos^{-1}(r_k/r_{\max}) \tag{9.11}$$

$$\phi_{k2} = \theta_k - \cos^{-1}(r_k/r_{\max}) + \pi, \tag{9.12}$$

we obtain

$$s_k = \frac{r_{\max}}{2}\left(e^{j\phi_{k1}} - e^{j\phi_{k2}}\right). \tag{9.13}$$

Figure 9.4 shows the procedure to find the two phases of ϕ_{k1} and ϕ_{k2} in the circle with radius of $r_{\max}/2$ for the constellation point of s_k. The real number of r_k is equal to the sum of two conjugate symmetric complex numbers of $\frac{1}{2}r_k \pm jy_k$ in the circle with radius of $\frac{1}{2}r_{\max}$, i.e., $\frac{1}{4}r_k^2 + y_k^2 =$

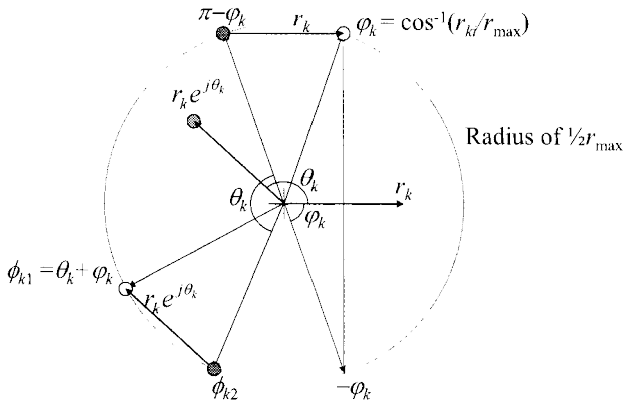

Figure 9.4. The procedure to find ϕ_{k1} and ϕ_{k2} for $s_k = r_k e^{j\theta_k}$. [Adapted from Ho and Cuei (2005)]

$\frac{1}{4}r_{\max}^2$. With $\varphi_k = \cos^{-1}(r_k/r_{\max})$, we obtain $\frac{1}{2}r_k \pm jy_k = \frac{1}{2}r_{\max}e^{\pm j\varphi_k}$. Figure 9.4 represents the two complex numbers of $\frac{1}{2}r_{\max}e^{\pm j\varphi_k}$ as two vectors in the phase angle of $\pm\varphi_k$ with $r_k = \frac{1}{2}r_{\max}e^{j\varphi_k} + \frac{1}{2}r_{\max}e^{-j\varphi_k}$. Alternatively, we may rewrite the summation as the difference of

$$r_k = \frac{1}{2}r_{\max}e^{j\varphi_k} - \frac{1}{2}r_{\max}e^{j(\pi-\varphi_k)}. \tag{9.14}$$

Figure 9.4 also shows the difference of Eq. (9.14) to find r_k. The signal of $s_k = r_k e^{j\theta_k}$ is a rotation of θ_k from r_k. If $e^{j\theta_k}$ is multiply to both sides of Eq. (9.14), we obtain the expression of Eq. (9.13) with ϕ_{k1} and ϕ_{k2} given by Eq. (9.11) and Eq. (9.12), respectively. In Fig. 9.4, the three vectors of r_k, $\frac{1}{2}r_{\max}e^{j\varphi_k}$, and $\frac{1}{2}r_{\max}e^{j(\pi-\varphi_k)}$ are rotated by an angle of θ_k to obtain $r_k e^{j\theta_k}$, $\frac{1}{2}r_{\max}e^{j\phi_{k1}}$, and $\frac{1}{2}r_{\max}e^{j\phi_{k2}}$, respectively.

All constellation points of Eq. (9.9) can be generated based on two phase modulators having the phases of Eqs. (9.11) and (9.12), respectively. The decomposition of a QAM signal or arbitrary quadrature signals into two phase-modulated signals was originated from Cox (1974) and Cox and Leck (1975). These types of linear amplification using nonlinear components (LINC) transmitter are very popular in wireless communications (Casadevall and Valdovinos, 1995, Shi and Sundstrom, 2000, Zhang et al., 2001). The two phases of Eqs. (9.11) and (9.12) drive the two phase modulators of Fig. 9.3 of the dual-drive Mach-Zehnder modulator.

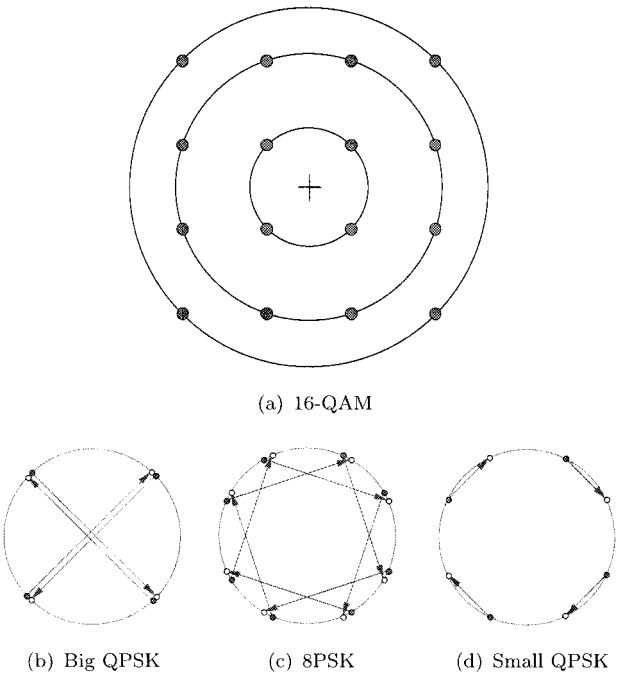

Figure 9.5. (a) 16-QAM constellation and its separation into two QPSK and an 8-PSK signals, (b), (c), (d) are the two phases of ϕ_1 (empty circles) and ϕ_2 (solid circles) to generate the 16-QAM signal. [Adapted from Ho and Cuei (2005)]

1.3 Generation of 16-QAM Signal

Figure 9.5(a) shows a 16-QAM constellation in a square grid. If the 16-QAM signal is generated by the conventional transmitter of Fig. 9.3(a), both $a(t)$ and $b(t)$ must be a four-level signal corresponding to the x- and y-axes of the constellation of Fig. 9.5(a). In the steady state for equal spacing, we get $a(t) = \pm 1, \pm 1/3$ and $b(t) = \pm 1, \pm 1/3$. If the push-pull modulator of Eq. (2.53) is used, the four amplitude levels of the drive signal for equal spacing $a(t)$ and $b(t)$ are $\pm V_\pi$ and $\pm 0.216 V_\pi$ after proper biasing.

Figures 9.5(b)-(d) show the phases of Eqs. (9.11) and (9.12) for the dual-drive Mach-Zehnder modulator to generate the constellation. Instead of representing all 16 constellation points in the same figure, Figure 9.5(a) separates the 16-QAM signal into two QPSK and one 8-PSK signals. Figures 9.5(b)-(d) are the corresponding ϕ_{k1} and ϕ_{k2} of all 16 points according to the separation of Fig. 9.5(a). The empty and solid

circles correspond to ϕ_{k1} and ϕ_{k2}, respectively. Figure 9.5(b) gives the QPSK signal of Fig. 9.5(a) with maximum amplitude of $r_{\max}$. For illustration purpose, the two closest points of Fig. 9.5(b) are the same but draw differently for the phases of two different signals. Figure 9.5(c) generates the 8-PSK signal of Fig. 9.5(a). Figure 9.5(d) gives the QPSK signal of Fig. 9.5(a) with the smallest amplitude.

From Figs. 9.5, the generation of a 16-QAM signal using a dual-drive Mach-Zehnder modulator requires the usage of a 16-level drive voltage and thus very complicated drive circuits. In the transmitter of Fig. 9.2, the two drive signals are two independent four-level drive signals corresponding to the x and y axis of Fig. 9.5(a). Compared with the conventional transmitter of Fig. 9.2, the simplification of the optical components using a single dual-drive Mach-Zehnder modulator creates a high complexity in the electronic driving circuits. With the allowance of higher modulator loss, as shown later, the number of drive levels can be reduced.

2. Transmitter of (D)QPSK Signals

DQPSK signal is by far the most popular multilevel signal for phase-modulated optical communications. The transmitter of (D)QPSK signal is considered here in more detail.

To generate the (D)QPSK signal using the conventional transmitter of Fig. 9.2, $V_1(t), V_2(t) = \pm V_\pi$ to provide the real and imaginary parts of Eq. (9.3) of ± 1, respectively. With the phase shift of $\pi/2$, the output of the transmitter becomes that of Eq. (9.3) with $s(t) = \pm\cos(\omega_c t) \pm \sin(\omega_c t)$.

A (D)QPSK signal can also be generated by the cascade of two phase modulators both driven by binary signal. One modulator provides a phase modulation of 0 and π similar to DPSK signal and may used a zero-chirp amplitude modulator of Eq. (2.53). Another modulator provides a phase modulation of $\pm\pi/2$ using a phase modulator. The amplitude ripples from the driving signal of the phase modulator transfers to the phase ripple. However, the amplitude ripples for the amplitude modulator does not transfer to to the phase ripple.

Alternatively, the (D)QPSK signal of Eq. (9.3) can also generate using a phase modulator driven by a four-level signal to give the phases of $\pm\pi/4$ and $\pm 3\pi/4$. However, the four-level signal is difficult to operate.

When the dual-drive modulator transmitter of Fig. 9.3 is used to generate (D)QPSK signals with a constellation of Fig. 9.1. Similar to that of Fig. 9.5(b), Fig. 9.6(a) is the trivial case of operating the dual-drive Mach-Zehnder modulator as a phase modulator when ϕ_1 and ϕ_2 are antipodal phases. The four phases of Fig. 9.1 are generated by a four-

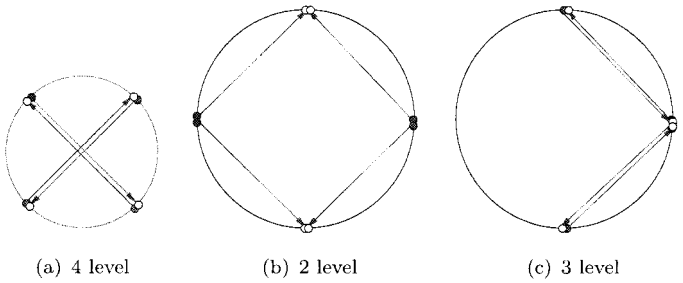

Figure 9.6. The generation of (D)QPSK signal using dual-drive modulator with (a) four-, (b) two-, and (c) three-level drive signal. [Adapted from Ho and Cuei (2005)]

level drive signal. The usage of a dual-drive Mach-Zehnder modulator as a phase modulator may not be an interesting application.

A (D)QPSK signal may be generated with higher loss but smaller number of levels if the four constellation points are generated with phases of ϕ_1 or ϕ_2 the same as one another. With only two values of ϕ_1 and ϕ_2, Figure 9.6(b) drives the dual-drive Mach-Zehnder modulator in Fig. 9.3 with a two-level drive signal. Figure 9.6(c) has three different values of ϕ_1 and ϕ_2 and requires a three-level drive signal. In Figs. 9.6(b) and (c), all phases of ϕ_1 and ϕ_2 are located in circle with the same diameter, representing the phase modulator with the same input signals. In Figs. 9.6, the vectors representing the output electric fields all have the same magnitude. The diameter of the circle of Fig. 9.6(a) is about $1/\sqrt{2}$ that of the circles of Figs. 9.6(b) and (c), requiring 1/2 the power at the input of the phase modulator to generate an output electric field of the same length. Alternatively, the schemes using two- and three-level drive signal have 3-dB extra loss more than that of Fig. 9.6(a).

The two level transmitter is for particular interested for it simplicity. Comparing Eq. (9.7) with (9.3), if the dual-drive modulator is driven with a binary signal such that $\exp(j\pi V_1/V_\pi) = \pm 1$ and $\exp(j\pi V_2/V_\pi) = \pm j$, all constellation points of Eq. (9.3) can be generated. The drive voltages are $V_1 = 0, V_\pi$ and $V_2 = \pm V_\pi/2$. The dual-drive modulator requires just a single bias control to ensure that the means of V_1 and V_2 have a difference of $V_\pi/2$. The peak-to-peak drive voltages of V_1 and V_2 are identical and equal to V_π.

In the two phase modulators of Fig. 9.3, the peak-to-peak drive voltages are proportional to the maximum phase difference of ϕ_1 or ϕ_2, respectively. The maximum phase difference of the 4-drive level of Fig. 9.6(a) is $3\pi/2$ and that of the two- and three-drive level of Figs. 9.6(b)

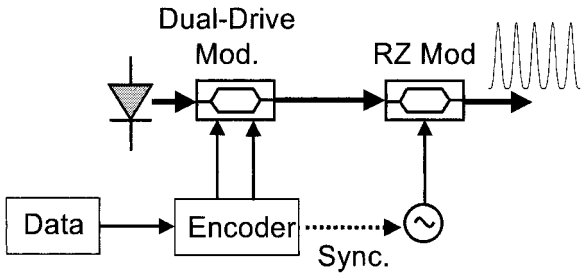

Figure 9.7. A RZ-(D)QPSK transmitter with a dual-drive Mach-Zehnder modulator followed by a RZ modulator. [From Ho and Cuei (2005), © 2005 IEEE]

and (c) is π. Both the peak-to-peak drive voltage and the number of drive levels are reduced in Figs. 9.6(b) and (c).

Figures 9.6 show the operation of the (D)QPSK transmitter in steady state when both ϕ_1 and ϕ_2 are in the correct phase angles. However, when the phases are in transition from one to another between consecutive transmitted symbols, the dynamic of the transmitter requires careful studies.

Similar to the conventional transmitter of Fig. 9.2, both the two- and three-level transmitters of Figs. 9.6(b) and (c) do not have constant intensity between consecutive symbols. Similar to Fig. 2.17 for return-to-zero (RZ)-DPSK, Figure 9.7 shows a RZ-(D)QPSK transmitter with the assumption of the usage of a dual-drive Mach-Zehnder modulator followed by a RZ modulator. In practice, the RZ modulator can either precede or follow the (D)QPSK generator. Without the RZ modulator, the transmitter of Fig. 9.7 gives non-return-to-zero (NRZ) (D)QPSK signal. The conventional transmitter of Fig. 9.2 can also be used in Fig. 9.7 to generate the (D)QPSK signals. The RZ modulator should be operated in the interval when the (D)QPSK signal generator is in steady state. Regardless of the transmitter types to generate the (D)QPSK signal, after the RZ modulator, the optical intensity is ideally a constant pulse train without ripple between symbols. However, the output signal of the dual-drive Mach-Zehnder modulator may have either overshoot and undershoot ripples.

Figures 9.8 show the eye-diagram of the drive signal and the optical intensity between the RZ modulator and the (D)QPSK transmitter. Figure 9.8(a) is the eye-diagram when the conventional transmitter of Fig. 9.2 is used with two two-level drive signals having a peak-to-peak drive voltage of $2V_\pi$. Using the dual-drive transmitter of Fig. 9.3, the

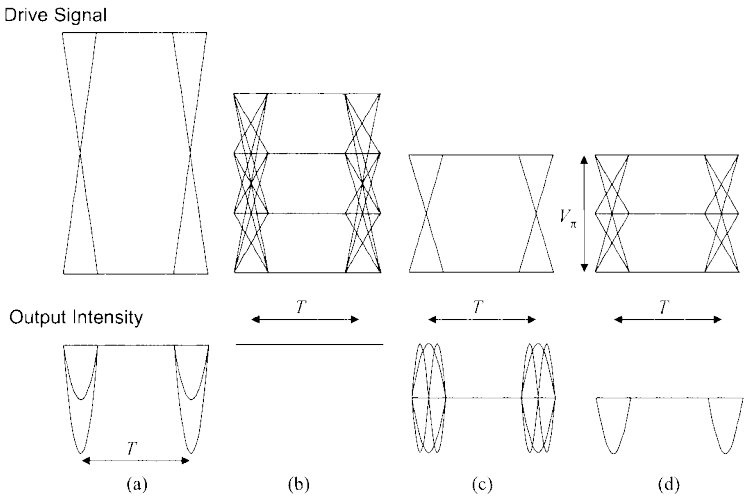

Figure 9.8. The eye-diagram of the drive signal and output intensity between two modulators of the transmitter of Fig. 9.7 when (a) the conventional transmitter of Fig. 9.2 and the dual-drive transmitter of Fig. 9.3 with (b) four-, (c) two-, and (d) three-level drive signals are used. [From Ho and Cuei (2005), © 2005 IEEE]

peak-to-peak drive voltage is reduced from $1.5V_\pi$ for four-level signal to V_π for two- and three-level drive signals.

The output intensity of the conventional transmitter has optical intensity ripples between consecutive symbols. With two or three levels of drive signal, the output intensity of the dual-drive Mach-Zehnder modulator also has ripples between consecutive symbols. The simplest two-level scheme of Figs. 9.6(b) and 9.8(c) has overshoot ripples doubling the output intensity. The ripples of the three-level signal of Fig. 9.8(d) with dual-drive transmitter are similar to that of Fig. 9.8(a) with conventional transmitter. For NRZ signal without RZ modulator, overshoot ripples are equivalent to short optical pulses that are particularly detrimental and potentially give high signal distortion due to fiber nonlinearities. Without the RZ modulator, two-level drive signals of Fig. 9.6(b) cannot be used for NRZ signals due to the overshoot ripples.

While Figs. 9.8 show the eye-diagram of the optical intensity, Figures 9.9 show the trace of the output electric field with both the real and imaginary parts. The four signal constellation points of Fig. 9.1 are shown in Fig. 9.9 as solid circles. The electric field of Fig. 9.9 other than the four signal constellation points occurs during the transition between consecutive (D)QPSK symbols. Other than Fig. 9.9(b) with all

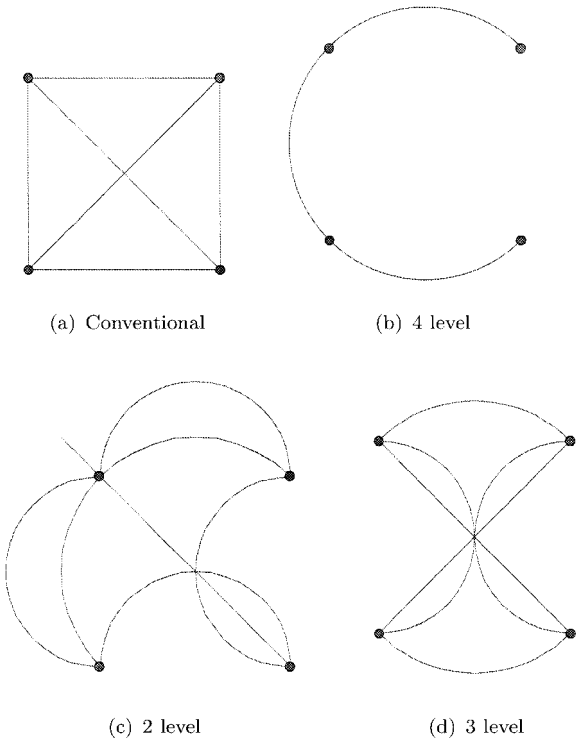

Figure 9.9. The electric field locus of a (D)QPSK signal generated using (a) conventional transmitter of Fig. 9.2, and dual-drive transmitter of Fig. 9.3 with (b) four-, (c) two-, and (d) three-level drive signals. [From Ho and Cuei (2005), © 2005 IEEE]

electric field in the same circle with equal distance to the origin (constant intensity), other traces show that the electric field has a wide range of variations. Those variations of electric field are equivalent to frequency chirp (Gnauck et al., 1991, Koyama and Oga, 1988).

In the conventional transmitter of Fig. 9.9(a), the electric field may pass through the origin and has an intensity equal to zero as shown in the optical intensity of Fig. 9.8(a). The electric field trace of the two-level signal of Figs. 9.6(b) and 9.8(c) shows a peak electric field about $\sqrt{2}$ of the signal points, corresponding to optical intensity ripples twice the steady-state intensity. The three-level signal of Fig. 9.9(d) has the same behavior as Fig. 9.9(a). Of course, the three-level signal of Fig. 9.9(d) has transition with constant intensity but all transitions of the conventional signal of Fig. 9.9(a) have ripples.

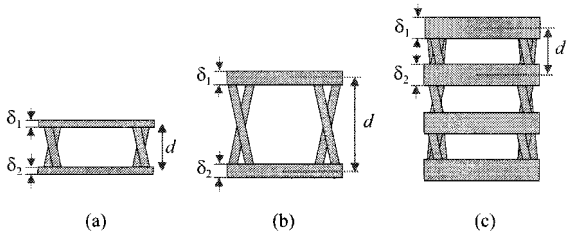

Figure 9.10. The increases of eye-spreading for a multi-level signal. [From Ho and Cuei (2005), © 2005 IEEE]

Figure 9.8 also shows the eye-diagram of the electrical drive signal to the dual-drive modulator with a peak-to-peak voltage of V_π. Similar to the conventional DQPSK transmitter of Fig. 9.2, for NRZ signals without the RZ modulator, the transmitter of Fig. 9.3 has intensity ripples between consecutive symbols. Together with the overshoot intensity ripples, phase jitter occurs between consecutive symbols. With an RZ modulator followed or preceded the DQPSK generator, both the intensity ripple and phase jitter can be eliminated. The RZ modulator has to be operated within the region when the DQPSK generator is in the steady state in the middle of its eye-diagram. In Fig. 9.8, the RZ modulator gives an RZ pulse having a duty-cycle of 50%. The drive signals of the dual-drive modulator must have a short rise- and fall-time to ensure that the both the overshoot ripple and phase jitter are outside the pulses generated by the RZ modulator.

The ripples of the drive signal transfer to the optical signal. With conventional transmitter of Fig. 9.2, no amplitude ripple of the drive signal transfers to phase ripple. Even when the drive signal has large ripple, the intensity ripple of the transmitted signal is compressed by the nonlinear transfer function of the modulator.

To generate the (D)QPSK signal of Figs. 9.1 using a phase modulator, the ripples from the drive signal increases by the transmitter. Figure 9.10 illustrates the increase of eye-spreading when two two-level signals are summed to a four-level signal. If the eye-spreading is defined as $\Delta_e = (\delta_1 + \delta_2)/d$, where δ_1 and δ_2 are the ripple (or spreading) in the upper and lower level, and d is the high of the eye-diagram, the eye-closure is $1 - \frac{1}{2}\Delta_e$ and the eye-penalty is equal to $10 \cdot \log_{10}\left(1 - \frac{1}{2}\Delta_e\right)$. From Fig. 9.10, when two two-level signals of Figs. 9.10(a) and (b) are summed to the four-level signal of Fig. 9.10(c), the eye-spreading is increased by a factor of three. When phase modulator is used to generate the (D)QPSK signal, the eye-spreading of the phase increases accordingly.

Table 9.1. The Transfer of Amplitude Ripples from Drive Signal to the Receiver for DQPSK Signals.

Schemes	Two-Level	Multi-Level	RZ Pulses	Received Signal
Four-Level	10%	30%	1.3%	47%
Two-Level	10%	Nil	31%	33%
Three-Level	Nil	10%	15%	16%
Conventional	10%	Nil	0.7%	0.6%

Table 9.1 shows the eye-spreading of Δ_e for all RZ-DQPSK transmitters discussed in this section and the conventional transmitter by assuming an "initial" eye-spreading of 10% for convenience. In the four-level transmitter, the initial 10% eye-spreading is increased to 30% as illustrate in Fig. 9.10. For QPSK signals without the differential operation, the spreading of the received signal is also equal to 30%. When the dual-drive modulator functions as a phase modulator, the RZ pulses at the output of the transmitter do not have eye-spreading but the DQPSK receivers have an eye-spreading of 47% due to phase distortion. The two-level transmitter provides a received signal spreading of about 33%, less than that of four-level transmitter. The internal operation of the two-level transmitter may be similar to the illustration of Fig. 9.10. For three-level transmitter, the eye-spreading is increased by a factor of 1.5. In conventional transmitter, ripples of the drive signal do not transfer to phase ripple but only small amplitude ripple. Table 9.1 shows that a drive signal ripple of 10% gives a received signal ripples less than 1%.

For the DQPSK transmitter using dual-drive modulator, the eye-spreading of the received signal increases almost linearly with the eye-spreading of the drive signal. For an eye-penalty less than 1 dB at the received signal, 41% eye-spreading is allowed, translating to a maximum eye-spreading of the two-level signal of 8.7% and 12.8% for four- and two-level transmitters, respectively. For an eye-penalty less than 0.5 dB, 22% eye-spreading is allowed, translating to a maximum eye-spreading of the two-level signal of 5.7% and 6.9% for four- and two-level transmitters, respectively.

As long as the electrical drive signal has very good quality and RZ modulator is used, the RZ-(D)QPSK transmitter using dual-drive modulator can generate mathematically the same signal as conventional transmitter. RZ-(D)QPSK signal broadens the bandwidth of the signal inversely proportional to the duty-cycle of the RZ pulses. Ripples or

eye-spreading transferred from the electrical drive signal are the major degradation using a phase modulator or dual-drive modulator to generate (D)QPSK signals.

Most DQPSK demonstrations used an integrated transmitter in Griffin and Carter (2002), Griffin et al. (2003), Zhu et al. (2004b), and Cho et al. (2003, 2004a,b). DQPSK signals were also generated by the cascade of practically two phase modulators driven by two binary sequences in Kim and Essiambre (2003), Tokle et al. (2004), Wree et al. (2003a), and Yoshikane and Morita (2004a,b, 2005).

3. Synchronous Detection of Multilevel Signals

Synchronous receiver with PLL to track the received phase gives the best receiver sensitivity. With large number of signal levels, synchronous receiver is usually 3-dB better than the corresponding asynchronous receiver. The multilevel quadrature signals may be M-ary PSK or QAM signals. Multilevel frequency-shift keying (FSK) signals do not provide good spectral efficiency and are not discussed here.

3.1 M-ary PSK Signal

The synchronous quadrature receiver of Fig. 3.4 can be used to detect the M-ary PSK signal of Eq. (9.1) where the M possible phases of $\theta_k = \pi(2k-1)/M, k = 1, 2, \ldots, M$ are used to carry the information. Assume that the receiver is limited by amplifier noise, when the phase of θ_k is the transmitted, the phase distribution is $p_{\Theta_n}(\theta - \theta_k)$, where $p_{\Theta_n}(\theta)$ is from Eq. (4.A.7) in Appendix 4.A. When Gray code is used, the bit error probability is equal to

$$p_e = \frac{1}{\log_2 M}\left[1 - \int_{-\pi/M}^{+\pi/M} p_{\Theta_n}(\theta)\mathrm{d}\theta\right]. \tag{9.15}$$

Using the series expansion of Eq. (4.A.12), the bit error probability is equal to

$$\begin{aligned} p_e &= \frac{1}{\log_2 M}\left\{1 - \frac{1}{M} - \frac{\sqrt{\rho_s}e^{-\rho_s/2}}{\sqrt{\pi}}\right. \\ &\quad \left. \times \sum_{m=1}^{\infty} \frac{\sin(m\pi/M)}{m}\left[I_{\frac{m-1}{2}}\left(\frac{\rho_s}{2}\right) + I_{\frac{m+1}{2}}\left(\frac{\rho_s}{2}\right)\right]\right\}. \end{aligned} \tag{9.16}$$

When $M = 2$ for binary PSK signal, the series of Eq. (9.16) is the same as that from Eq. (4.A.16), or $\frac{1}{2}\mathrm{erfc}(\sqrt{\rho_s})$ of Eq. (3.78).

The series summation of Eq. (9.16) is difficult to evaluate from Appendix 4.A. The minimum Euclidean distance between the two closest

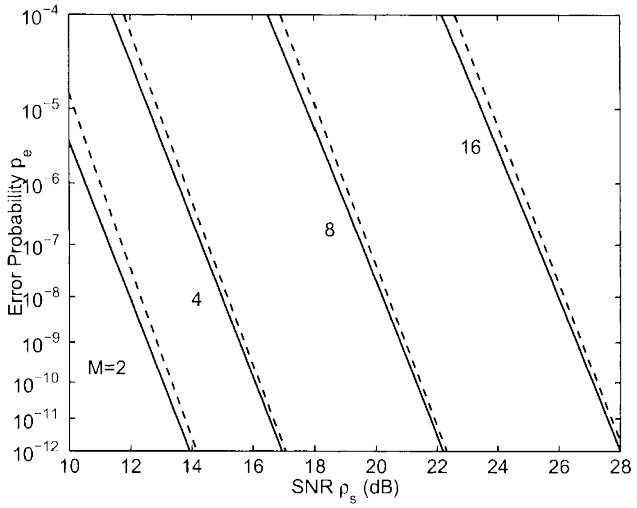

Figure 9.11. The bit-error probability of M-ary PSK signal. The solid lines is exact results from the series of Eq. (9.16) and the dashed lines are the approximation from Eq. (9.17).

signal points is $\sqrt{2}A \sin \pi/M$ and the error probability is approximately equal to

$$p_e \approx \frac{2}{\log_2 M} \text{erfc}\left(\sqrt{\rho_s} \sin \frac{\pi}{M}\right). \tag{9.17}$$

Figure 9.11 shows the bit-error probability calculated using the exact series summation of Eq. (9.16) and the approximation of Eq. (9.17). For $M \geq 8$, the approximation of Eq. (9.17) is very accurate. For binary PSK, the exact error probability is given by Eq. (3.78). For QPSK signals, the constellation is the same as Fig. 9.1 with the combination of two sets of antipodal phases. The minimum distance is reduced by $\sqrt{2}$ as compared with binary PSK. The correct probability is when both quadratures are correct of $(1 - p_e)^2$, where p_e the error probability of binary PSK of Eq. (3.78) with $\sqrt{2}$ less power. The exact symbol error probability for QPSK is $1 - (1 - p_e)^2$, and the bit error probability is

$$\frac{1}{4}\text{erfc}\sqrt{\frac{\rho_s}{2}}\left[1 - \frac{1}{4}\text{erfc}\sqrt{\frac{\rho_s}{2}}\right]. \tag{9.18}$$

QPSK signal is about 3-dB worse than binary PSK signal but half the bandwidth and half the noise. QPSK and binary PSK signals require the same SNR per bit.

The error probability of Eq. (9.16) was first derived by Prabhu (1969).

3.2 Quadrature Amplitude Modulation

The M-ary QAM signal of Eq. (9.4) can also also be detected using the synchronous quadrature receiver of Fig. 3.4. The average energy per symbol of the QAM signal of Eq. (9.4) is

$$E_{\rm av} = \frac{2A^2}{M}\sum_{k=1}^{\sqrt{M}}\left(-\sqrt{M}+2k-1\right)^2 = \frac{2A^2}{3}(M-1). \tag{9.19}$$

For each dimension, the symbol error probability is

$$p_x = p_y = \left(1-\frac{1}{\sqrt{M}}\right)\operatorname{erfc}\sqrt{\frac{A^2}{2\sigma_n^2}}. \tag{9.20}$$

The symbol error probability for QAM signal is when both quadrature components are correct of $1-(1-p_x)(1-p_y)$. The bit error probability is

$$\begin{aligned} p_e &= \frac{2}{\log_2 M}\left(1-\frac{1}{\sqrt{M}}\right)\operatorname{erfc}\sqrt{\frac{3\rho_s}{2(M-1)}} \\ &\quad\times\left[1-\frac{1}{2}\left(1-\frac{1}{\sqrt{M}}\right)\operatorname{erfc}\sqrt{\frac{3\rho_s}{2(M-1)}}\right]. \end{aligned} \tag{9.21}$$

For $M=4$, the error probability is the same as that of Eq. (9.18) for QPSK signal.

In high SNR, we obtain

$$p_e \approx \frac{2}{\log_2 M}\left(1-\frac{1}{\sqrt{M}}\right)\operatorname{erfc}\sqrt{\frac{3\rho_s}{2(M-1)}}. \tag{9.22}$$

Figure 9.12 shows the bit-error probability of M-ary QAM signals for $M=4,8,16,32$, and 64. The 4-QAM signal is the same as QPSK signal of Eq. (9.18). The required SNR of the signal increases with the number of levels in the constellation. For $M=8$ and 32, the error probability of Eq. (9.21) is modified for the non-square constellation.

QPSK signal was demonstrated using different types of synchronous receiver (Derr, 1990, Kahn et al., 1992, Norimatsu et al., 1992). QPSK signal was analyzed by Barry and Kahn (1992) and Yamazaki and Emura (1990) in detail. An intradyne receiver was proposed by Derr (1992) using signal processing for demodulation.

M-ary FSK was also analyzed by Jeromin and Chan (1986) and demonstrated in Alexander et al. (1990). Although M-ary FSK signals

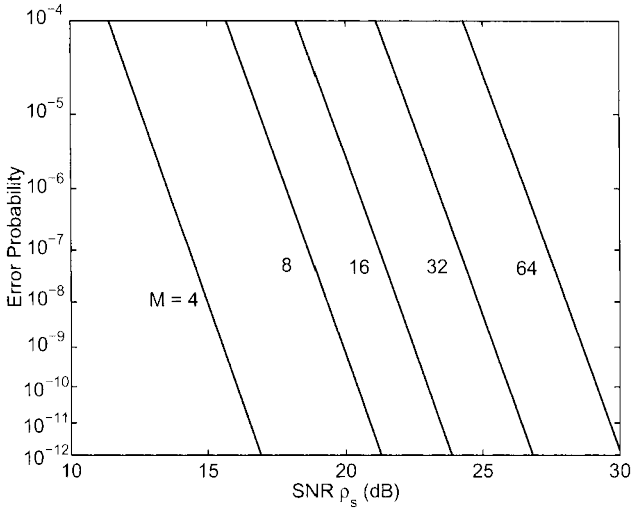

Figure 9.12. The bit-error probability of M-ary QAM signal.

do not have good spectral efficiency, using more bandwidth to obtain better performance, M-ary FSK signals can achieve very small SNR per bit.

Both M-ary PSK and QAM signals for large M have very small tolerance to laser and nonlinear phase noise. Using the 16-QAM signal of Fig. 9.5(a) as an example, laser phase noise spreads out the phase of all constellation point equally. Separated by an angle of $\pi/4$, the middle 8-PSK signal is affected the most by the laser phase noise. If the system is dominated by laser phase noise, the optimal signal constellation is four concentric circles of QPSK signal or two concentric circles of 8-PSK signal with equal angles between two adjacent constellation points.

For system with nonlinear phase noise, the amount of nonlinear phase noise depends on the distance of the signal to the origin. The big QPSK in 16-QAM signal of Fig. 9.5(a) has nine times larger nonlinear phase noise than the small QPSK signal. For system with large nonlinear phase noise, the optimal signal constellation may have QPSK signal at larger amplitude but 8-PSK signal at smaller amplitude, differed with conventional signal design.

Currently, QAM signal with more than four levels is rarely used for optical communications. Of course, subcarrier multiplexing may use high-level QAM signals for cable modem or digital video applications (Phillips and Darcie, 1997, Way, 1998). High-speed subcarrier multi-

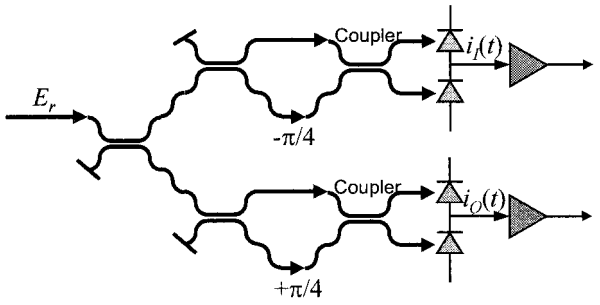

Figure 9.13. Direct-Detection Receiver for DQPSK Signals.

plexing may also use high-level and high-speed QAM signals (Chen and Way, 2004, Hui et al., 2002, Urick et al., 2004). Equivalently an 8-QAM signal, DQPSK signal can also use together with amplitude-shift keying (ASK) signal (Hayase et al., 2004, Miyazaki and Kubota, 2004).

4. Direct-Detection of DQPSK Signal

DPSK signal is demodulated using a direct-detection receiver based on the interferometric receiver of Fig. 1.4(c). DQPSK receiver uses two asymmetric Mach-Zehnder interferometers for the differential phase of each quadrature component. Direct-detection DQPSK receiver is the most popular receiver for multilevel phase-modulated optical communications from as Table 1.3.

4.1 Receiver Structure and Ideal Performance

Figure 9.13 shows the direct-detection receiver for DQPSK signals. The received electric field of E_r is splitted into two paths of $\pm E_r/\sqrt{2}$ and passing through two asymmetric interferometers with phase difference of $\pi/2$. The two interferometers also have a path difference of the symbol time of T. With the received signal of $E_r = Ae^{j\phi_s(t)} + n(t)$, assuming ideal 3-dB coupler and balanced receiver, the photocurrent of upper branch is

$$i_I(t) = \frac{A^2}{2}\cos[\phi_s(t) - \phi_s(t-T) + \pi/4] + \text{noise terms.} \tag{9.23}$$

the photocurrent of the lower branch is

$$i_Q(t) = \frac{A^2}{2}\cos[\phi_s(t) - \phi_s(t-T) - \pi/4] + \text{noise terms.} \tag{9.24}$$

Without noise, a phase difference of $\phi_s(t) - \phi_s(t-T) = 0°$ gives an output of $i_I(t) = i_Q(t) = A^2/2$. A phase difference of 90° gives

an output of $i_I(t) = A^2/2$ and $i_Q(t) = -A^2/2$. A phase difference of $\phi_s(t) - \phi_s(t-T) = 180^\circ$ gives an output of $i_I(t) = i_Q(t) = -A^2/2$. A phase difference of -90° gives an output of $i_I(t) = -A^2/2$ and $i_Q(t) = A^2/2$. The signs of both $i_I(t)$ and $i_Q(t)$ can map to the detected bits of the data.

In the simplest method, the error probability of DQPSK signal can be analyzed using the series expansion of Eq. (4.A.18). When the transmitted phases of consecutive symbols are the same, error occurs when the received differential phase is outside $\pm\pi/4$ or

$$\begin{aligned} p_e &= \frac{1}{2}\left(1 - \int_{-\pi/4}^{+\pi/4} p_{\Delta\Theta_n}(\theta)\mathrm{d}\theta\right) \\ &= \frac{3}{8} - \frac{\rho_s e^{-\rho_s}}{4}\sum_{m=1}^{\infty}\frac{\sin(m\pi/4)}{m}\left[I_{\frac{m-1}{2}}\left(\frac{\rho_s}{2}\right) + I_{\frac{m+1}{2}}\left(\frac{\rho_s}{2}\right)\right]^2. \end{aligned} \tag{9.25}$$

Alternatively, a DQPSK signal is the same as the correlated binary signals of Sec. 3.3.6 with correlation coefficient of $\rho = 1/\sqrt{2}$. The error probability is that of Eq. (3.119)

$$p_e = Q(a,b) - \frac{1}{2}e^{-(a^2+b^2)/2}I_0(ab) \tag{9.26}$$

with

$$a = \sqrt{\rho_s\left(1 - \sqrt{1/2}\right)}, \qquad b = \sqrt{\rho_s\left(1 + \sqrt{1/2}\right)}. \tag{9.27}$$

Equivalently speaking, the error probability of Eq. (9.26) is the same as that of DPSK signal with phase error of Eq. (4.10) when the phase error is $\theta_e = 45^\circ$.

The error probability of Eq. (9.26) ignores amplifier noise from orthogonal polarization by assuming a polarized receiver. If the amplifier noise from orthogonal polarization is included, the error probability is the same as that of Eq. (4.11) for DPSK signal with the parameters a and b given by Eq. (9.27).

Figure 9.14 shows the error probability of DQPSK signal as a function of SNR ρ_s. The error probability with and without amplifier noise from orthogonal polarization is almost the same. The error probability of binary PSK and QPSK signals of Eqs. (3.78) and (9.18) is also shown for comparison. The error probability for DPSK signal of Eq. (3.105) is also shown in Fig. 9.14.

For an error probability of 10^{-9}, DQPSK signal requires a SNR of $\rho_s = 17.9$ dB, 4.9 dB larger than the requirement of DPSK signal

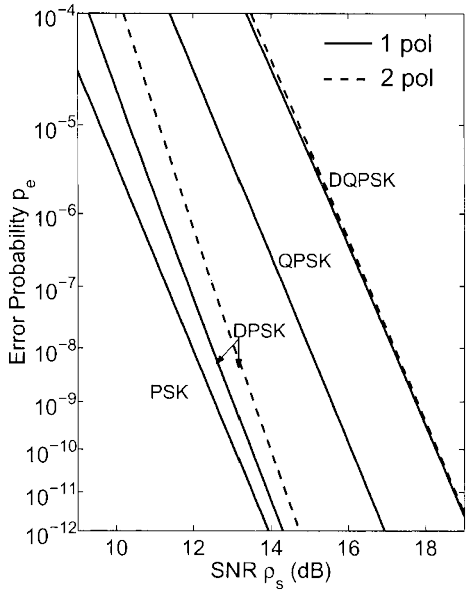

Figure 9.14. The error probability of binary and quaternary PSK and DPSK signals.

for a heterodyne receiver, or 4.5 dB larger than an unpolarized direct-detection receiver. In term of SNR per bit, DQPSK signal requires 1.9 dB larger than DPSK signal with heterodyne receiver. DQPSK signal is 2.2 dB worse than QPSK signal.

For M-ary DPSK signal, the signal is demodulated according to the phase difference of $\Delta\Theta_n = \Theta_n(t) - \Theta_n(t-T)$. For $M \geq 8$, both Θ_n and $\Theta_n(t-T)$ can assume to be both Gaussian distributed. The phase variance of $\Delta\Theta_n$ is twice that of $\Theta_n(t)$ and $\Theta_n(t-T)$. The error probability is the same as that of Eq. (9.17) but with twice the noise. For $M \geq 8$, the bit-error probability for M-ary DPSK signal is approximately given by

$$p_e \approx \frac{2}{\log_2 M} \text{erfc}\left(\sqrt{\frac{\rho_s}{2}} \sin\frac{\pi}{M}\right). \tag{9.28}$$

Recently, there are proposals to use 8-level DPSK signal to improve the spectral efficiency (Han et al., 2004, Ohm, 2004).

4.2 Impairment to DQPSK Signals

Similar to DPSK signal as analyzed in Chapter 4, DQPSK signal is degraded by both interferometer phase error and laser phase noise.

Similar to DPSK signal of Chapter 5, DQPSK signal is also degraded by nonlinear phase noise.

Interferometer Phase Error

The performance of DPSK signal with interferometer phase error is discussed in Sec. 4.2.1 based on an equivalent correlation coefficient. Without going into details, with phase error, the bit-error probability for DQPSK signal is

$$\begin{aligned} p_e &= \frac{1}{2}\Bigg\{Q_1(a_+,b_+) - \frac{1}{2}e^{-(a_+^2+b_+^2)/2}I_0(a_+b_+) \\ &\qquad +Q_1(a_-,b_-) - \frac{1}{2}e^{-(a_-^2+b_-^2)/2}I_0(a_-b_-)\Bigg\}, \\ &\qquad a_\pm = \sqrt{\rho_s\left[1-\cos\left(\frac{\pi}{4}\pm\theta_e\right)\right]}, \\ &\qquad b_\pm = \sqrt{\rho_s\left[1+\cos\left(\frac{\pi}{4}\pm\theta_e\right)\right]}, \end{aligned} \tag{9.29}$$

where θ_e is the phase error of the asymmetric interferometer.

From the two terms of Eq. (9.29), due to the phase error, the two adjacent points of the signal constellation of the DQPSK signal have different correlation coefficients. The correlated angles to the adjacent points are increased (corresponding to a_+ and b_+) or decreased (corresponding to a_- and b_-) by the phase error of θ_e from $\pi/4$. In practice, the two asymmetric Mach-Zehnder interferometers of Fig. 9.13 may have two phase errors. The error probability is the average of the error probability given by Eq. (9.29) when the two phase errors are used in Eq. (9.29).

Figure 9.15 shows the SNR penalty as a function of phase error for DQPSK signals for polarized DQPSK receiver. The SNR penalty from Fig. 4.3 for DPSK signal with phase error is also shown for comparison. The SNR penalty is calculated for a BER of 10^{-9}, corresponding to a required SNR of 13 and 17.9 dB for DPSK and DQPSK signals, respectively.

The curve of SNR penalty of a DQPSK signal in Fig. 9.15 has insignificant difference with the corresponding curves in Kim and Winzer (2003, Fig. 3), Bosco and Poggiolini (2003, Fig. 2), Bosco and Poggiolini (2004b, Fig. 2), and Winzer and Kim (2003, Fig.5) (required the adjusting of x-axis).

For the same SNR penalty, the DQPSK signal is about 2.7 times more sensitive to the phase error than the DPSK signal, more or less the same ratio as the experimental and simulated results in Kim and

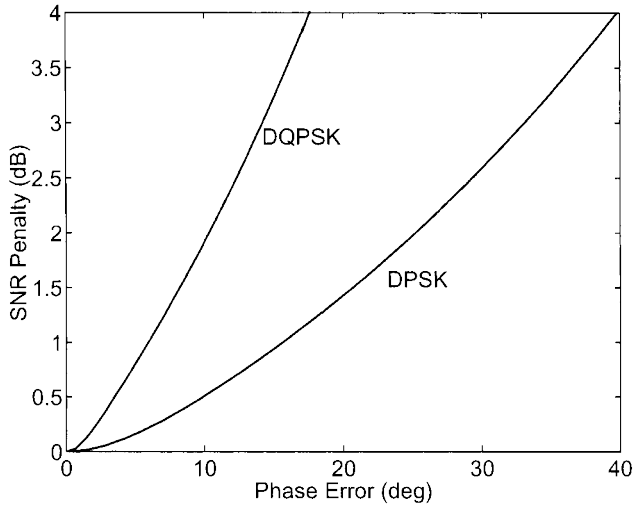

Figure 9.15. SNR penalty as a function of interferometer phase error for DQPSK signals. [From Ho (2004a), © 2005 IEEE]

Winzer (2003). The phase error for a SNR penalty of 1 dB is about 6° (or 1.7% of 360°) for a DQPSK signal, the same as the ratio of mismatched frequency to the symbol rate of Kim and Winzer (2003, Fig. 3) by simulation. The measurement of Kim and Winzer (2003) shows a larger penalty than that of Fig. 9.15 due to non-ideal signal source (Winzer and Kim, 2003). The analysis for interferometer phase error to DQPSK signal here follows that in Ho (2004a).

Nonlinear and Laser Phase Noise

DQPSK signal is affected by both nonlinear and laser phase noise. As shown in Fig. 5.15, the impact of nonlinear phase noise to DPSK signal does not have the same model as that of laser phase noise. However, unlike DPSK signal, the impact of nonlinear and laser phase noise to DQPSK can use the same model and determine by the variance of the phase noise.